a 

AEROELASTIC TAILORING FOR COMPOSITE ADAPTIVE WINGLETS

Natsuki Tsushima[1,2], Ryo Higuchi[2] & Tomohiro Yokozeki[2]

[1]Kyushu University, 744 Motooka, Nishi-Ward, Fukuoka, 819-0395, Japan
[2]The University of Tokyo, 7-3-1 Hongo, Bunkyo, Tokyo, 113-8656, Japan

Abstract

This study investigates aeroelastic tailoring of composite winglets using a full-aircraft, trim-coupled aeroelastic framework, with particular focus on the influence of laminate coupling characteristics on aerodynamic performance and structural integrity. Unlike conventional laminate optimization approaches based on lamination parameters, which require post-processing for stacking sequence reconstruction and often complicate strength evaluation, the present study introduces a super-ply-based laminate representation. This approach enables direct control of stiffness distribution while maintaining manufacturable stacking sequences and enabling consistent structural strength assessment within the same optimization framework. A geometrically nonlinear aeroelastic model combining the vortex lattice method and a corotational composite shell formulation is employed to capture the interaction between aerodynamic loads, structural deformation, and aircraft trim. The results show that bending-dominated laminates lead to excessive wash-out deformation and significant aerodynamic penalties. In contrast, shear-dominant and bend–twist coupled laminates effectively suppress deformation and achieve more than 10 counts of induced drag reduction. It is further demonstrated that the relationship between aerodynamic performance and structural integrity depends on the direction of bending–torsion coupling. Depending on the laminate configuration, aerodynamic performance improvement can either increase or alleviate structural loading, indicating that the aeroelastic trade-off is not universal. These findings highlight the importance of coupling direction in composite aeroelastic tailoring and demonstrate the effectiveness of the proposed super-ply-based framework for multi-disciplinary design of adaptive winglets.

Keywords: Aeroelasticity, Winglets, Composites, Adaptive Structures

1. Introduction

Wingtip devices are widely used to improve aerodynamic efficiency by reducing the strength of wingtip vortices and the associated induced drag. Conventional winglets, however, are generally designed as fixed geometric devices optimized for a limited set of flight conditions. Their aerodynamic benefit can therefore be reduced, or even accompanied by undesirable structural penalties, when the aircraft operates away from the design point, such as during high-load maneuvers. This limitation is particularly important for light aircraft and high-load maneuvering configurations, where the wingtip structure is subjected to significant aerodynamic loading and where the interaction between winglet aerodynamics, trim, and structural deformation can become non-negligible.

Composite structures offer a promising route to overcome this limitation through aeroelastic tailoring. By exploiting the anisotropic stiffness of laminated composites, structural deformation can be directed toward beneficial passive shape changes, such as load-dependent twist or wash-out. This concept is especially attractive for adaptive winglets because the winglet is located in a region where aerodynamic loads, moment arms, and tip-vortex-related flow structures are strongly coupled. A properly tailored composite winglet can therefore act not only as an aerodynamic device, but also as a passive load-redistribution mechanism that adapts to different flight conditions without active actuation.

Previous studies on aeroelastic tailoring have demonstrated that composite anisotropy can be used to modify bending, torsion, and coupled deformation characteristics of flexible lifting surfaces. In

many design studies, however, winglet performance is evaluated primarily from a rigid aerodynamic viewpoint or through isolated wing models. Such approaches do not fully capture aircraft-level effects, including longitudinal trim, elevator deflection, tail load, and the redistribution of aerodynamic loads caused by structural deformation. For high-load maneuver conditions, these effects become particularly important because the aerodynamic optimum predicted by a rigid model may differ from the actual aeroelastic response of the full aircraft.

The present study investigates aeroelastic tailoring for composite adaptive winglets using a full-aircraft trim-coupled aeroelastic framework. This study extends a previously developed aeroelastic framework [1-4] to include composite structural modeling and focuses on the tailoring of winglet geometries for optimized aerodynamic performance across a broader flight envelope. The analysis combines a vortex-lattice aerodynamic model with a geometrically nonlinear corotational shell finite element formulation. Composite skins, spars, ribs, and sandwich structures are modeled using classical laminate theory, allowing ply-level stress recovery and structural safety assessment. The target configuration is a representative General Aviation (GA) high-load light-aircraft model equipped with a blended composite winglet. The model includes simplified horizontal and vertical tail lifting surfaces, control surfaces, a lumped fuselage/payload mass, and a fixed winglet geometry. The winglet geometry is kept constant in order to isolate the effect of composite stiffness tailoring.

As a baseline investigation, rigid-aerodynamic and aeroelastic trim analyses are first conducted at 1G cruise and 4G pull-up conditions. The 4G case is selected as a representative high-load maneuver condition that provides sufficiently large winglet loading while avoiding the strongly separated regime expected in more severe 5G conditions. The rigid-aerodynamic results provide a reference for the load distribution and trim state of the fixed geometry, whereas the aeroelastic results quantify the effects of structural deformation, flying twist, and structural safety margins. These baseline results are then used to motivate the composite tailoring study of the winglet laminate.

The objective of this paper is not to reproduce a specific certified aircraft, but to establish a practical analysis and design framework for composite adaptive winglets under aircraft-level trim constraints. The main contributions of this study are: (1) construction of a full-aircraft composite wing-winglet model suitable for trim-coupled aeroelastic analysis; (2) comparison of rigid-aerodynamic and aeroelastic trim characteristics at 1G and 4G conditions; (3) evaluation of passive deformation, flying twist, and structural safety of the baseline composite winglet; and (4) formulation of a composite tailoring strategy for adaptive winglets based on manufacturable laminate candidates.

In addition, most existing studies on composite aeroelastic tailoring rely on lamination parameters (LPs) to represent stiffness properties. While LPs provide a convenient continuous design space, they require an inverse process to recover discrete stacking sequences, which can introduce ambiguity and complicate structural strength evaluation. In contrast, practical design requires both stiffness tailoring and direct assessment of structural safety. To address this limitation, the present study adopts a super-ply-based laminate representation, where the laminate is parameterized by physically interpretable ply groups while preserving manufacturability and enabling direct stress and failure evaluation. This approach allows consistent consideration of aerodynamic performance and structural integrity within a unified aeroelastic design framework.

2. Aeroelastic Analysis Framework

This study employs a medium-fidelity aeroelastic analysis framework for evaluating trim-coupled aerodynamic and aeroelastic characteristics of composite wing-winglet configurations. The framework combines a vortex-lattice aerodynamic model with a geometrically nonlinear composite shell finite element model. The same numerical framework can also be extended to unsteady vortex-lattice-based flutter analysis when dynamic stability is considered. In the present paper, the baseline aerodynamic and static aeroelastic characteristics are primarily evaluated using steady VLM, while the UVLM-based flutter capability is retained in the formulation for possible stability assessment.

The objective of the framework is to capture the aircraft-level interaction among aerodynamic loading, longitudinal trim, composite structural deformation, and structural safety. The viscous-inviscid interaction model developed in the authors' separate work is not used in the present study. Therefore, the present aerodynamic analysis is interpreted as an inviscid reference for comparing trim-coupled load redistribution and aeroelastic deformation.

2.1 Structural Model

Two coordinate systems are used to describe the coupled flight and aeroelastic problem, as shown in Fig.1. The global frame *G* is an inertial frame used to define the aircraft translational velocity and attitude. The body-fixed frame *B* is attached to the aircraft reference point, which is located at the leading edge of the wing root. The structural finite element mesh and aerodynamic panel geometry are defined in the body-fixed frame.

The transformation from the global frame to the body-fixed frame is expressed by the direction cosine matrix $\mathbf{C}_{GB}$. A vector $\mathbf{v}_G$ defined in the global frame is transformed into the body-fixed frame as

$$\mathbf{v}_B = \mathbf{C}_{GB}\mathbf{v}_G \tag{1}$$

In the present trim analysis, the primary aircraft attitude variable is the body pitch angle θ. The freestream velocity vector is transformed into the body-fixed frame and used as the inflow condition for the vortex-lattice calculation. The elevator deflection δ_e is introduced as the longitudinal control variable for satisfying the pitching-moment equilibrium.

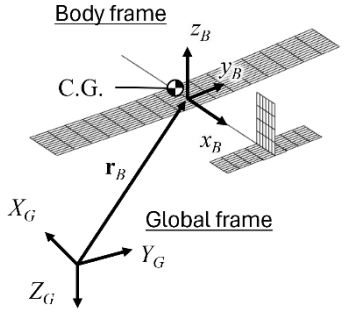


Figure 1 – Coordinate frames.

2.2 Geometrically Nonlinear Composite Shell Model

The structural response of the wing-winglet configuration is modeled using a geometrically nonlinear shell finite element formulation. A four-node quadrilateral (QUAD4) shell element based on the Mixed Interpolation of Tensorial Components (MITC4) formulation [5] is implemented to reduce shear locking in thin-walled composite structures. Large displacements and rotations are considered using a corotational approach [3, 4, 6], in which the rigid-body motion of each element is separated from the local elastic deformation.

The nonlinear static equilibrium equation of the structure is written as

$$\mathbf{R}(\mathbf{u}) = \mathbf{F}_{ext} - \mathbf{F}_{\text{int}}(\mathbf{u}) = 0 \tag{2}$$

where $\mathbf{u}$ is the structural displacement vector, $\mathbf{F}_{ext}$ is the external load vector, and $\mathbf{F}_{int}$ is the internal force vector evaluated from the corotational element formulation. The external loads include aerodynamic forces mapped from the lifting-surface model and, when required, inertial or maneuver loads. The nonlinear equilibrium equation is solved iteratively until the structural and aero-structural coupling residuals satisfy the prescribed convergence tolerances.

For static aeroelastic analysis, the structural deformation modifies the aerodynamic surface geometry. The aerodynamic forces are then recomputed on the deformed configuration, and the coupling iteration is repeated until convergence. This procedure enables the framework to capture trim-coupled static aeroelastic deformation under high-load maneuver conditions.

2.3 Composite Laminate and Sandwich Modeling

Composite skins, spars, ribs, and winglet components are represented as laminated shell structures. The equivalent laminate stiffness is obtained from Classical Laminate Theory (CLT) [7]. The relation between the membrane force resultants, bending moment resultants, mid-surface strains, and curvatures is written as

$$\begin{Bmatrix} \mathbf{N} \\ \mathbf{M} \end{Bmatrix} = \begin{bmatrix} \mathbf{A} & \mathbf{B} \\ \mathbf{B} & \mathbf{D} \end{bmatrix} \begin{Bmatrix} \boldsymbol{\varepsilon}_0 \\ \boldsymbol{\kappa} \end{Bmatrix} \tag{3}$$

where **N** and **M** are the membrane force and bending moment resultants, respectively. The vectors $\boldsymbol{\varepsilon}_0$ and $\boldsymbol{\kappa}$ denote the mid-surface strain and curvature, and **A**, **B**, and **D** are the extensional, extension-bending coupling, and bending stiffness matrices.

Sandwich laminates are modeled by explicitly defining carbon-epoxy face sheets and a lightweight core layer in the laminate stacking sequence. This approach preserves ply-level information for stress recovery and structural safety assessment while retaining an equivalent shell representation suitable for repeated aeroelastic analyses.

LPs [7] provide a compact continuous representation of composite stiffness and are useful for interpreting the design space of aeroelastic tailoring. However, the present full-aircraft problem involves sandwich-core thickness, ply-level stress recovery, and structural safety constraints. Therefore, the final tailoring study adopts a manufacturable laminate-candidate approach rather than a full lamination-parameter retrieval procedure. The resulting laminate designs are evaluated through their equivalent stiffness, passive deformation, trim response, and structural safety.

2.4 Aerodynamic Model

Aerodynamic loads in the baseline trim analysis are evaluated using the Vortex Lattice Method (VLM) [8]. The lifting surfaces, including the main wing, winglet, horizontal tail, and vertical tail, are discretized into quadrilateral aerodynamic panels placed on their mean camber surfaces. Each panel is associated with a bound vortex element, and the circulation distribution is determined by enforcing the non-penetration boundary condition at the control points.

The steady aerodynamic force vector is evaluated from the resulting circulation distribution and is then transferred to the structural finite element mesh. The present VLM model is inviscid and does not include profile drag, flow separation, or stall effects. Therefore, the raw axial-force coefficient obtained from VLM is not interpreted as the total aircraft drag. In this study, the VLM results are used primarily to compare lift distribution, induced-load trends, trim conditions, and aeroelastic load redistribution under a consistent inviscid framework.

2.5 Aero-Structural Coupling

The structural and aerodynamic meshes are non-matching. Therefore, displacement and load transfer between the two meshes is performed using a thin-plate spline (TPS) interpolation [9]. Structural displacements are interpolated to the aerodynamic control points to update the deformed aerodynamic surface. Conversely, aerodynamic panel forces are mapped back to the structural nodes as equivalent nodal forces using the principle of virtual work.

The static aeroelastic solution is obtained through an iterative coupling procedure. At each coupling iteration, aerodynamic loads are computed on the current aerodynamic geometry, transferred to the structural mesh, and used to update the structural deformation. The deformed structural geometry is then mapped back to the aerodynamic grid. This procedure is repeated until the change in structural displacement or the aero-structural residual becomes sufficiently small.

2.6 Trim and Pull-Up Analysis

The full-aircraft trim condition is determined by enforcing the force and pitching-moment equilibrium. For a prescribed load factor n, the target lift is defined as

$$L_{\text{target}} = nW \tag{4}$$

where W is the aircraft weight. The trim variables are the body pitch angle θ and the elevator deflection δ_e, collected in the vector

$$\mathbf{S} = \begin{bmatrix} \theta & \delta_e \end{bmatrix}^T \tag{5}$$

The trim residual vector is defined as

$$\mathbf{f}(\mathbf{S}) = \begin{bmatrix} L(\mathbf{S}) - L_{\text{target}} \\ M_y(\mathbf{S}) \end{bmatrix} \tag{6}$$

where L is the total aerodynamic lift and M_y is the pitching moment about the aircraft center of gravity. The trim solution is obtained by solving

$$\mathbf{f}(\mathbf{S}) = \mathbf{0} \tag{7}$$

using a nonlinear least-squares procedure with prescribed bounds on θ and δ_e.

Two trim conditions are considered in the baseline study: a 1G cruise condition and a 4G pull-up maneuver condition. The 4G case is selected as the representative high-load maneuver condition because it produces significant winglet loading while remaining less severe than the 5G case, where separated-flow effects may become dominant for the NACA 2412 section. The same trim formulation is applied to both rigid-aerodynamic and aeroelastic analyses, enabling direct comparison between the rigid and deformed configurations.

2.7 Structural Safety Assessment and Tailoring Parameters

For aeroelastic cases, ply-level stresses are recovered from the laminate strain state of each shell element. The structural safety of the composite components is evaluated using a Tsai-Wu failure index. The maximum failure index and the corresponding margin of safety are used as structural feasibility metrics for the baseline and tailored designs.

The present tailoring study focuses on the composite stiffness distribution of the winglet while keeping the external winglet geometry fixed. The geometric parameters of the winglet, including cant angle, leading-edge sweep angle, and toe angle, are prescribed in the baseline model. The tailoring variables are associated with manufacturable laminate candidates, including ply orientation groups, face-sheet stiffness distribution, and sandwich-core thickness. This formulation allows the influence of composite stiffness tailoring on passive winglet deformation, trim response, and structural safety to be evaluated without introducing a lamination-parameter retrieval loop.

3. Full-Aircraft Composite Wing–Winglet Model

A full-aircraft aeroelastic model is constructed to investigate the trim-coupled aerodynamic and structural response of composite adaptive winglets. The model represents a GA high-load light-aircraft configuration and is not intended to reproduce a specific certified aircraft. Instead, it provides a simplified but physically consistent platform for evaluating the interaction between winglet aerodynamics, aircraft trim, and composite aeroelastic deformation.

3.1 Overall Aircraft Configuration

The full-aircraft model consists of a main wing, a blended winglet, horizontal and vertical tail surfaces, and a simplified fuselage representation, as shown in Fig. 2. The fuselage and onboard systems are modeled as a lumped point mass located near the wing root leading edge. The aerodynamic lifting surfaces are modeled explicitly, while the fuselage aerodynamic contribution is neglected.

The horizontal and vertical tails are modeled as lifting surfaces within the vortex-lattice framework to provide longitudinal and directional stability, as well as control authority. Elevator deflection is introduced as the primary control variable for trim analysis. The resulting configuration captures the essential coupling between wing, tail, and winglet required for full-aircraft trim analysis. Fundamental parameters of the baseline aircraft are summarized in Table 1.

3.2 Wing and Winglet Geometry

The main wing has a span of 8.0 m with a linearly tapered planform from a root chord of 1.63 m to a tip chord of 0.90 m. The leading-edge sweep and dihedral angles are set to zero, and the wing uses a NACA 2412 airfoil section along the span. The winglet is modeled as a blended winglet with a smooth geometric transition from the wing tip. The winglet geometry is defined by target parameters at the tip and interpolated along the winglet span. The key parameters are listed in Table 1.

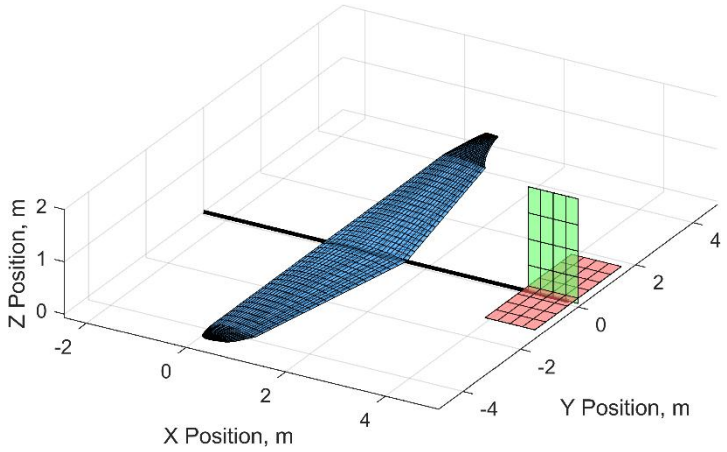


Figure 2 – Representative aircraft model.

Table 1. Properties of baseline aircraft model.

Property	Value	Unit
Wing		
Root chord	1.63	m
Taper ratio	0.55	--
Span	8.0	m
Airfoil	NACA2412	--
Winglet		
Tip chord	0.27	m
Length	0.88	m
Cant angle	30.0	deg
Toe angle	0.0	deg
Leading-edge sweep angle	45.0	deg
Airfoil	NACA2412	--
Horizontal tail		
Chord length	1.0	m
Taper ratio	1.0	--
Span	3.0	m
Airfoil	Flat plate (thickness 50 mm)	--
Vertical tail		
Chord length	1.0	m
Taper ratio	1.0	--
Span	2.0	m
Airfoil	Flat plate (thickness 50 mm)	--
Fuselage		
Weight	600	kg

In the present study, the winglet geometry is fixed in order to isolate the effect of composite stiffness tailoring. The selected winglet configuration has a cant angle of 30°, a leading-edge sweep angle of 45°, and a toe (twist) angle of 0°. The length of the winglet is 0.88 m, and the chord tapers linearly from 0.90 m at the root to 0.27 m at the tip. The winglet geometry represents a moderately canted blended winglet configuration suitable for evaluating passive aeroelastic deformation and load redistribution under high-load conditions.

3.3 Structural Modeling

The structural model of the wing-winglet system consists of upper and lower composite skins, a main spar, ribs, and a winglet tip cap. The structure is modeled using shell finite elements based on the formulation described in Section 2.

The main spar is located at 25% chord and extends continuously from the wing root to the winglet. The ribs are distributed along the span to represent internal load paths and structural support. The

rib positions are assigned at equal arc-length intervals along the main wing and winglet, while ensuring that a rib is placed at the wing–winglet junction. As a result, eight ribs are placed along the main wing and one rib along the winglet, with uniform spacing in terms of structural arc-length. The skin panels, spar, and ribs are modeled as laminated composite shells with prescribed thickness and material properties.

Sandwich construction is used for selected components, where carbon-epoxy face sheets are combined with a lightweight core made of PVC foam. The carbon fiber reinforced plastic (CFRP) used in this study is assumed to be T800/S3900-2B, a high-strength carbon/epoxy prepreg widely used in aerospace structures. The material exhibits high longitudinal stiffness and strength along the fiber direction, combined with relatively low transverse stiffness, making it suitable for exploiting anisotropic aeroelastic tailoring effects. The material properties are listed in Table 2. Layups of each component for the baseline design are summarized in Table 3. This modeling approach enables the evaluation of both structural stiffness and failure behavior through ply-level stress recovery.

The total mass of the full-aircraft model is 675.38 kg, including a 600 kg lumped mass representing the fuselage and payload. The center of gravity is located at X_{cg} = 0.517 m (from the reference origin). The reference aerodynamic quantities are defined as S_{ref} = 9.27 m^2 and *MAC* (mean aerodynamic chord) = 1.112 m. These values are computed from the geometric model of the wing-winglet system. The trim and aeroelastic analyses are performed at a freestream velocity of 80 m/s. Two flight conditions are considered: a 1G cruise trim condition and a 4G pull-up maneuver condition. These conditions are used to evaluate both the aerodynamic baseline and the aeroelastic response of the composite winglet.

The structural discretization is refined sufficiently to capture wing bending and winglet deformation, while maintaining computational efficiency for repeated trim and aeroelastic analyses.

Table 2. Material properties of CFRP (T800/S3900-2B) and PVC foam.

Property	Value	Unit
CFRP		
Axial modulus E_1	153	GPa
Transverse modulus E_2	8.30	GPa
Poisson's ratio ν_{12}	0.34	--
Shear modulus G_{12}	4.03	GPa
Density ρ	1,550	kg/m^3
Ply thickness	0.150	mm
PVC foam		
Young's modulus E	0.1	GPa
Poisson's ratio ν	0.4	--
Density ρ	80.0	kg/m^3

Table 3. Composite Layups of baseline aircraft model.

Property	Outer skin	Core	Inner skin
Main Wing Skin	CFRP [45_2 / -45_2 / 90_3 / 0_2]	PVC foam (5 mm)	CFRP [0_2 / 90_3 / -45_2 / 45_2]
Winglet Skin (Baseline)	CFRP [$\pm45_2$]	PVC foam (3 mm)	CFRP [$\mp45_2$]
Main Spar	CFRP [$\pm45_2$ / 90_{15}]	PVC foam (10 mm)	CFRP [90_{15} / $\mp45_2$]
Winglet Spar	CFRP [±45]	PVC foam (6 mm)	CFRP [∓45]
Ribs (Main & Winglet)	CFRP [±45 / 0 / 90]	PVC foam (5 mm)	CFRP [90 / 0 / ∓45]

3.4 Aerodynamic Model Discretization

The lifting surfaces are discretized using a structured vortex-lattice grid defined on the mean camber surfaces. The spanwise direction is divided into 32 sections, with the first 16 corresponding to the

main wing and the remaining 16 to the winglet. The chordwise direction is discretized into 12 panels. This discretization allows the spanwise load distribution and winglet contribution to be evaluated consistently between rigid aerodynamic and aeroelastic analyses.

The aerodynamic mesh is coupled to the structural mesh through the TPS interpolation described in Section 2. The resulting mapping ensures consistent transfer of displacements and aerodynamic loads between the structural and aerodynamic models.

4. Baseline Aeroelastic Characteristics

4.1 Rigid Aerodynamic Trim Characteristics

A rigid aerodynamic trim analysis was first conducted for both 1G cruise and 4G pull-up conditions in order to establish a baseline reference. At the 1G condition, the aircraft is trimmed at a small negative body pitch angle (-1.2°) with a moderate elevator deflection (2.4°). The resulting total lift coefficient of the full wing (wing-winglet system) is approximately $C_L \approx 0.17$, indicating that the aerodynamic loading is relatively low and distributed mainly over the main wing.

At the 4G pull-up condition, the required lift increases to four times the aircraft weight, resulting in a trimmed angle of attack of approximately $\alpha \approx 11.2°$. The elevator deflection changes sign (-2.0°) to balance the pitching moment generated by the high lift. The spanwise load distribution illustrate a smooth decay from the wing root toward the tip, with a gradual transition into the winglet region, as shown in Fig. 3.

These rigid aerodynamic results provide a consistent reference for evaluating the influence of structural deformation on trim and load redistribution.

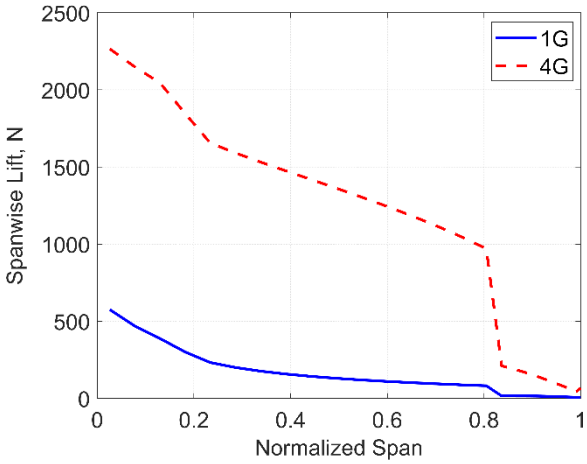


Figure 3 – Spanwise lift distribution for rigid aerodynamic analysis at 1G and 4G.

4.2 Aeroelastic Response at 1G and 4G

Figure 4 compares the aeroelastic deformation and spanwise lift distributions at 1G and 4G conditions. The aeroelastic trim analysis at the 1G condition shows that structural deformation is very small. The wingtip vertical displacement is approximately 7.6 mm, corresponding to less than 0.2% of the semi-span. The associated twist angle is about −0.21°. As a result, the aerodynamic coefficients and trim variables are nearly identical to those obtained from the rigid analysis. The static margin remains approximately 5%, and the structural safety margin is very high (MoS ≈ 46), indicating that the structure is far from critical loading. These results confirm that the aeroelastic effects are negligible at the 1G condition, and the configuration behaves essentially as a rigid aircraft. Therefore, the 1G case is regarded as a quasi-rigid baseline for subsequent analysis.

In contrast, the aeroelastic effects become clearly observable at the 4G pull-up condition. The wingtip vertical displacement reaches approximately 0.10 m, corresponding to about 2% of the semi-span. The associated twist angle increases to −0.54°, indicating the presence of bending-torsion coupling under high aerodynamic loading. Although the deformation level is still moderate and well below the range typically associated with strongly nonlinear geometric effects, it is sufficient to modify the aerodynamic characteristics and trim condition.

Although the overall spanwise load distributions in Figs. 3 and 4 appear visually similar, a quantitative

comparison reveals a subtle but important difference. This difference arises from the combined effect of aeroelastic deformation and trim adjustment. At the 1G condition, structural deformation is minimal (tip twist ≈ −0.21°), and the aeroelastic case produces a slightly higher total lift than the rigid case (3.563 kN vs. 3.561 kN). This increase is mainly attributed to a small increase in effective angle of attack due to deformation, while trim variations remain negligible. As a result, the aerodynamic response is essentially identical to the rigid configuration. In contrast, at the 4G condition, aeroelastic deformation becomes more pronounced, with a larger nose-down twist (≈ −0.54°). This deformation tends to reduce the local angle of attack, particularly near the wingtip and winglet region, leading to a tendency toward local lift relief. At the same time, the trim condition is modified, requiring a higher angle of attack and different elevator deflection to satisfy equilibrium. This trim adjustment partially compensates for the deformation-induced lift reduction. As a result, the total lift in the aeroelastic case is slightly higher than that in the rigid case (26.31 kN vs. 26.24 kN), while the spanwise load distribution exhibits subtle redistribution. This indicates that the observed difference is governed by the competing effects of deformation-induced load relief and trim-induced lift compensation.

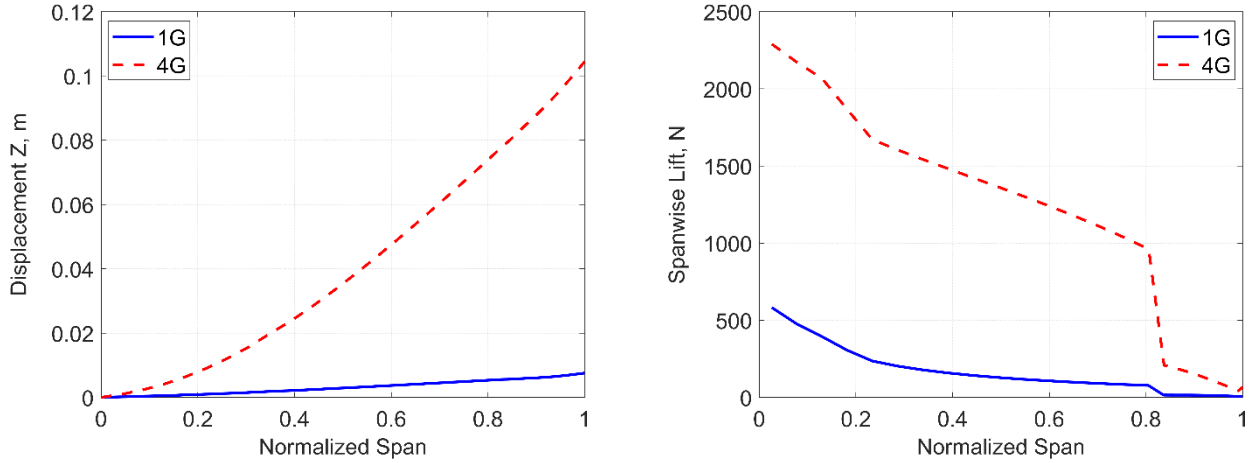


Figure 4 – Aeroelastic deformation (left) and spanwise lift distribution (right) at 4G condition.

4.3 Structural Safety Evaluation

The structural safety assessment shows that the maximum Tsai-Wu failure index at 4G is approximately 0.17, corresponding to a margin of safety of about +3.4. The critical element is located near the wing root region, approximately five elements away from the root along the spanwise direction and close to the mid-chord location. This region experiences a combination of high bending moment and structural compliance, leading to the maximum stress.

Although the structure remains well within the safe limit, the load increase from 1G to 4G results in a significant growth of stress levels, indicating that structural effects become increasingly important in high-load conditions. This trend indicates that structural constraints will become increasingly influential in the subsequent composite tailoring optimization.

In addition to structural safety considerations, it is also important to interpret how these load levels are associated with the aeroelastic behavior observed in the previous sections. The comparison between rigid and aeroelastic analyses leads to the following key observations:

1. At the 1G condition, aeroelastic deformation is negligible, and the aerodynamic characteristics are essentially identical to those of a rigid configuration.
2. At the 4G condition, moderate deformation occurs, leading to noticeable changes in trim and load distribution.
3. Although the deformation level remains relatively small (approximately 2% of the semi-span), it is sufficient to influence aerodynamic performance, particularly in the wing tip and winglet region.

These results demonstrate that aeroelastic effects must be considered when evaluating winglet performance under high-load maneuver conditions. The established baseline provides a consistent reference for the subsequent composite tailoring study.

5. Aeroelastic Tailoring of Winglet

5.1 Effect of Aeroelastic Tailoring on Winglet Performance

The effect of aeroelastic tailoring on the winglet performance was first evaluated through a comparative analysis between a bending-dominated baseline configuration and tailored laminate designs. Figure 5 shows the drag polar, twist response, and structural margin for the three representative configurations. The baseline configuration, consisting of a bending-dominated cross-ply laminate, exhibits significant wash-out deformation as the lift increases. At a flight velocity of 135 m/s and lift coefficient $C_L \approx 1.0$, the tip twist reaches approximately -2.77°, indicating a substantial loss of aerodynamic effectiveness. In contrast, the tailored configurations significantly mitigate the wash-out deformation. Both the bending-twist coupled laminate and the shear-dominant laminate, denoted as Tailored (-45°) and Tailored (Shear), reduce the magnitude of twist to approximately -1.82° and -1.62°. This reduction in deformation directly leads to improvement in aerodynamic performance. As shown in Fig. 5, the induced drag is reduced by more than 10 drag counts (11.0 drag counts with Tailored -45° and 11.9 drag counts with Tailored Shear) compared to the baseline configuration. This clearly demonstrates that aeroelastic tailoring does not merely alter structural stiffness, but actively controls the aeroelastic deformation to recover aerodynamic performance.

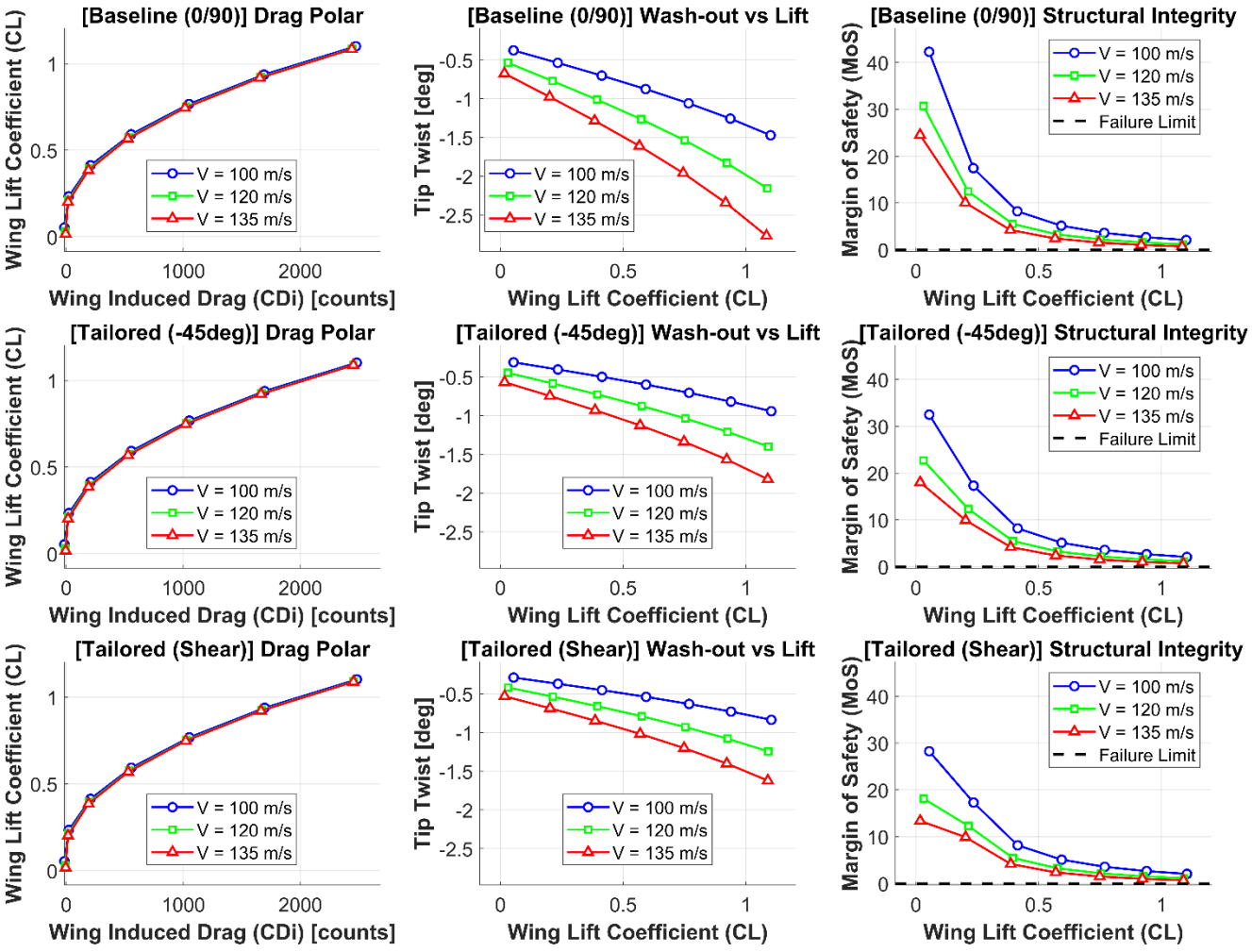


Figure 5 – Comparative drag polars, twist distributions, and structural margins.

5.2 Aeroelastic Characteristics and Sensitivity in Design Space

To further investigate the relationship between laminate design and aeroelastic response, a parametric sweep was performed over the laminate design space defined by the morphing (r_{morph}: off-axis coupling) ratio and bending-dominated (r_{bend}) ratio. The shear-dominated (r_{shear}: ±45°) ratio is subject to the constraint:

$$r_{morph} + r_{bend} + r_{shear} = 1 \tag{8}$$

Figure 6 shows the L/D, twist, and margin of safety distributions as functions of the laminate parameters for two morphing angles. The L/D maps in Fig. 6 exhibit a smooth and inclined distribution, indicating a clear dependence of aerodynamic performance on the laminate composition. Higher aerodynamic performance is achieved in regions where the contribution of shear-dominant plies is sufficiently large, while increasing the bending-dominated component leads to a gradual reduction in aerodynamic efficiency.

The corresponding tip twist maps in Fig. 6 reveal a strong correlation between laminate composition and aeroelastic deformation. In particular, increasing the proportion of shear-dominant plies (r_{shear}) effectively suppresses the wash-out deformation, whereas bending-dominated laminates (r_{bend}) lead to larger twist. This behavior can be explained by the bending-twist coupling governed by the D26 stiffness component, which couples spanwise bending deformation with torsional response. As the proportion of off-axis plies ($\pm 45°$) increases, the magnitude of D26 is enhanced, allowing effective control of aeroelastic twist. It should be noted that the interpretation of the coupling terms depends on the coordinate system. While D16 and D26 are defined in the laminate coordinate system, the dominant coupling mechanism in the present winglet configuration corresponds to the coupling between spanwise bending deformation and torsional response. Therefore, the aeroelastic twist is primarily governed by the effective contribution of D26 under the adopted structural and aerodynamic coordinate definitions.

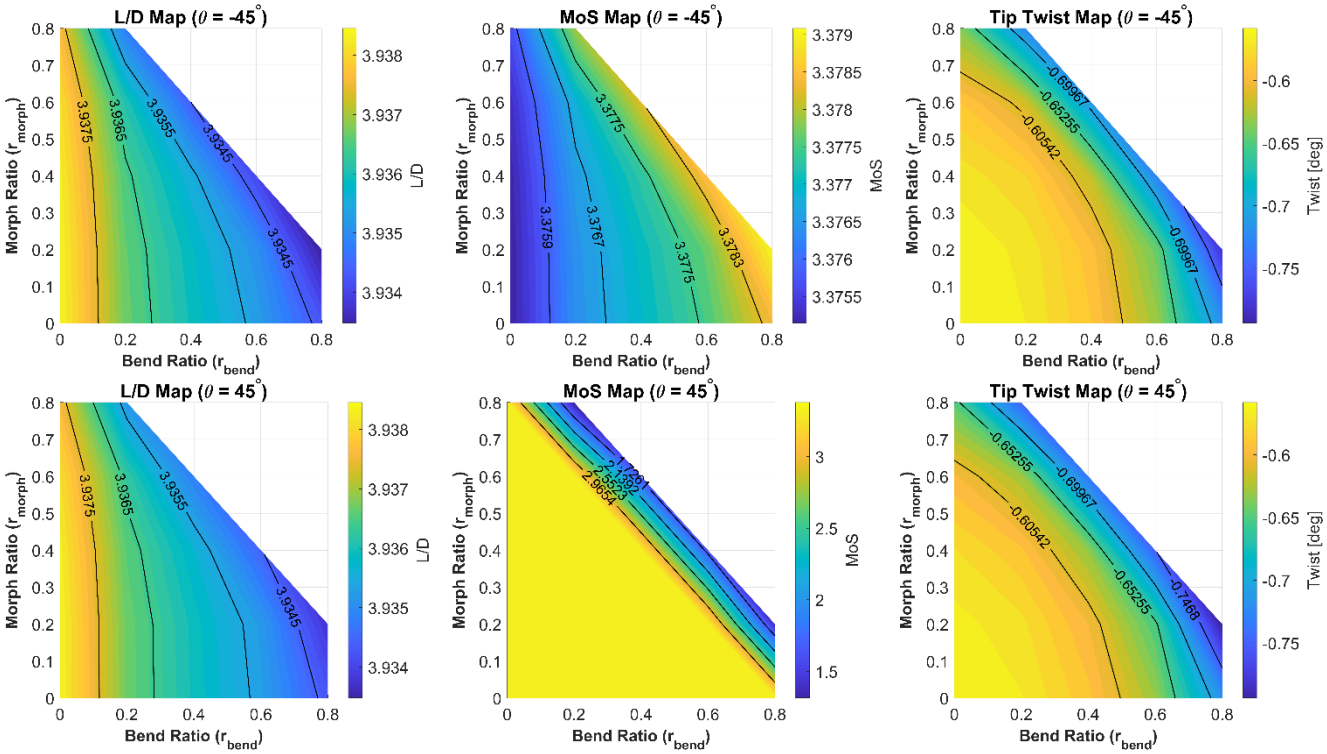


Figure 6 – Design parameter space showing L/D, tip twist, and margin of safety as functions of morphing and bending ratios for two morphing angles.

5.3 Aeroelastic Trade-off Between Performance and Structural Integrity

While the aerodynamic performance improves with tailoring, the relationship between aerodynamic efficiency and structural response is strongly influenced by the direction of bending-torsion coupling. Figure 7 provides a more direct physical interpretation of the aeroelastic response by visualizing the relationship between deformation (twist and displacement) and aerodynamic performance. As shown in Fig 7, for the -45° laminate configuration, regions with reduced wash-out (smaller negative twist) are associated with higher L/D but lower margin of safety. In this case, improving aerodynamic

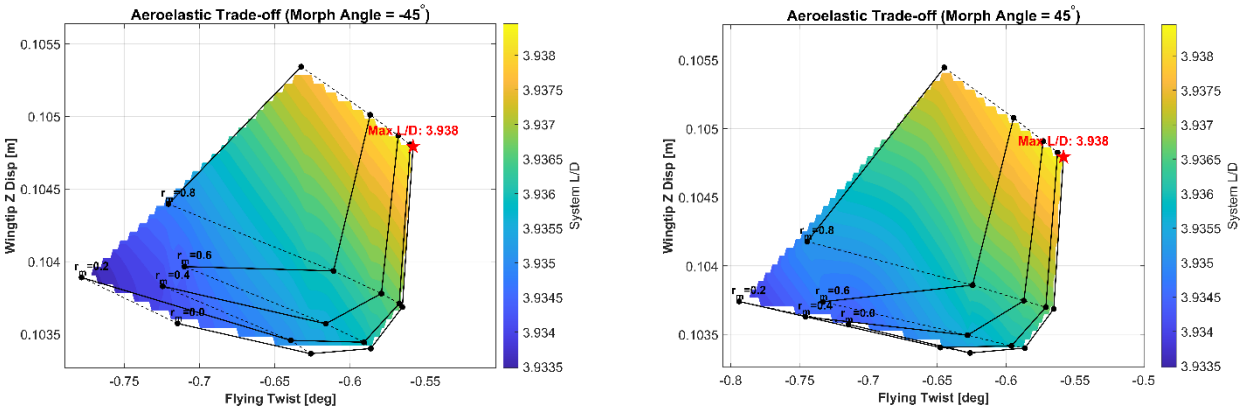


Figure 7 – Aeroelastic response space showing the relationship between tip twist, wingtip displacement, and aerodynamic performance (L/D) for the two morphing angles.

efficiency inevitably increases the structural load. This behavior can be understood physically as follows. When the wash-out deformation is suppressed, the winglet maintains a higher effective angle of attack, resulting in increased lift generation at the tip region. This increased lift produces a larger bending moment at the winglet root, thereby raising the structural load and reducing the available margin of safety. In contrast, for the +45° configuration, the highest aerodynamic performance is observed in the shear-dominated region, where the margin of safety is also maximized. In this case, the wash-out tendency alleviates load concentration near the wing root, resulting in reduced structural demand. These results indicate that the aeroelastic trade-off between performance and structural integrity is not universal, but depends fundamentally on the direction of bending–torsion coupling introduced by the laminate design. Therefore, the design problem is not simply to maximize aerodynamic performance, but to identify a configuration that balances aerodynamic and structural requirements based on the coupling characteristics. This behavior clearly demonstrates that winglet tailoring is inherently a multi-disciplinary design problem.

5.4 Implications for Winglet Structures Design

The present results provide important insights into the fundamental differences between wing and winglet structural design. In conventional wing design, laminate configurations are often optimized for bending stiffness to withstand the dominant aerodynamic loads. However, when such bending-oriented design concepts are directly applied to winglet structures, the lack of sufficient torsional stiffness leads to severe aeroelastic deformation and degraded aerodynamic performance.

The results of this study show that winglet structures require a different design philosophy. Rather than prioritizing bending stiffness alone, it is essential to provide sufficient torsional rigidity through shear-dominant laminates in order to control aeroelastic deformation. Furthermore, the present results demonstrate that the direction of bending–torsion coupling plays a crucial role in determining whether aerodynamic performance improvement leads to increased or alleviated structural loading. In other words, the role of composite tailoring in winglets is not to maximize stiffness in a single direction, but to achieve a balanced stiffness distribution that enables effective control of the aeroelastic response.

6. Conclusion

This study presented an aeroelastic tailoring framework for composite winglets using a full-aircraft, trim-coupled aeroelastic model. A super-ply-based laminate representation was introduced to enable direct manipulation of composite stiffness while preserving manufacturable stacking sequences and allowing consistent structural strength evaluation. This approach overcomes limitations of conventional lamination parameter-based methods, particularly in handling structural safety within an aeroelastic design context.

The results demonstrate that bending-dominated laminates lead to excessive wash-out deformation and degraded aerodynamic performance, while shear-dominant and bend–twist coupled laminates effectively suppress deformation and achieve more than 10 counts of induced drag reduction. It was further shown that the relationship between aerodynamic performance and structural loading is not

universal, but depends strongly on the direction of bending–torsion coupling. In the −45° configuration, performance improvement increases structural loading, whereas in the +45° configuration, aerodynamic and structural objectives can be aligned. These findings reveal that aeroelastic behavior is governed not only by stiffness magnitude but also by the directional characteristics of composite anisotropy. As a result, the conventional assumption of a fixed trade-off between aerodynamic efficiency and structural integrity does not necessarily apply to tailored composite winglets.

The present study demonstrates that super-ply-based aeroelastic tailoring provides a practical and physically interpretable framework for multi-disciplinary design of adaptive winglets, bridging the gap between theoretical laminate optimization and engineering implementation.

7. Contact Author Email Address

Corresponding author: Natsuki Tsushima, ntsushima@aero.kyushu-u.ac.jp

8. Copyright Statement

The authors confirm that they, and/or their company or organization, hold copyright on all of the original material included in this paper. The authors also confirm that they have obtained permission, from the copyright holder of any third party material included in this paper, to publish it as part of their paper. The authors confirm that they give permission, or have obtained permission from the copyright holder of this paper, for the publication and distribution of this paper as part of the ICAS proceedings or as individual off-prints from the proceedings.

Acknowledgement

This work was conducted under the financial support of the Grant-in-Aid for Scientific Research (No. 24K17450) by Japan Society for the Promotion of Science.

References

[1] Soneda K, Tsushima N, Yokozeki T and Imamura T, Longitudinal aeroelastic flight simulations of active morphing aircraft with corrugated structures, AIAA Journal, Vol. Published Online Nov. 18 No. pp, 2025.

[2] Tsushima N, Arizono H and Tamayama M, Geometrically nonlinear flutter analysis with corotational shell finite element analysis and unsteady vortex-lattice method, Journal of Sound and Vibration, Vol. 520 No. pp 116621, 2022.

[3] Tsushima N, Tamayama M, Arizono H and Makihara K, Geometrically nonlinear aeroelastic characteristics of highly flexible wing fabricated by additive manufacturing, Aerospace Science and Technology, Vol. 117 No. pp 106923, 2021.

[4] Tsushima N, Yokozeki T, Su W and Arizono H, Geometrically nonlinear static aeroelastic analysis of composite morphing wing with corrugated structures, Aerospace Science and Technology, Vol. 88 No. pp 244-257, 2019.

[5] Bathe K-J, Finite element procedures, Prentice Hall, Pearson Education, Inc., New Jersey, US, 2006.

[6] Khosravi P, Ganesan R and Sedaghati R, Corotational non-linear analysis of thin plates and shells using a new shell element, International Journal for Numerical Methods in Engineering, Vol. 69 No. 4 pp 859-885, 2007.

[7] Jones RM, Mechanics of composite materials, McGraw-Hill, New York, NY, 1975.

[8] Katz J and Plotkin A, Low-speed aerodynamics, Cambridge University Press, Cambridge, UK, 2001, 230-447.

[9] Smith MJ, Hodges DH and Cesnik CES, Evaluation of computational algorithms suitable for fluid-structure interactions, Journal of Aircraft, Vol. 37 No. 2 pp 282-294, 2000.